Implicit computational method for compressible flows with high and low Mach numbers

K. Aoki[1], S. Ushijima[2], D. Toriu[1], and H.Itada[1]

[1] Kyoto University, Civil and Earth Resources Engineering, Kyoto, 615-8540, Japan
[2] Prof., Kyoto University, ACCMS, Kyoto, 606-8501, Japan

*Corresponding author : aoki.kazuma.34z@st.kyoto-u.ac.jp

Abstract

This paper presents a new computational method for compressible flows with both high and low Mach numbers. In this method, the principal governing equations, such as the equation of mass, momentum and internal energy, are described with conservation forms, which are discretized with finite volume method (FVM) on a collocated grid system. In particular, since the special implicit method (C-ISMAC method) is applied to these governing equations, their convection terms can be estimated with higher-order TVD schemes in addition to the larger time increment Δt compared with the usual explicit methods that decreases computational time of our method.

The proposed computational method was applied to the shock wave problems with high Mach numbers as well as the natural convection flows driven by non-uniform temperatures with low Mach numbers. It was shown that the conservation of mass and other physical properties are sufficiently satisfied and that the predicted results are in good agreement with the theoretical values and calculated results reported by other researchers.

Keywords : compressible fluid, FVM, implicit method, Mach number, natural convection

Introduction

In this paper, a numerical method is investigated to predict compressible flows for high Mach numbers in addition to low Mach numbers. In order to construct such prediction methods, it is necessary to capture accurately shock discontinuity due to shock waves with high Mach numbers as well as to predict the compressible flows with low Mach numbers affected by large pressure or temperature differences.

To propose such computational method, the basic ideas used in the computations for incompressible fluids are employed: the numerical procedures in collocated grid system, special implicit method applicable to higher-order schemes in convection terms. Thus, the main numerical procedures are described as follows:

1). The governing equations are described in the conservative forms and the convection and diffusion terms are discretized with finite volume method (FVM).

2). As a result, the mass conservation law is satisfied accurately in the present computational method compared with the usual finite difference methods (FDM) based on non-conservative forms.

3). The employed implicit method (C-ISMAC method [Ushijima and Nezu (2002)]) enables us to utilize the higher-order TVD schemes and to use larger time increment Δt than explicit methods. Thus, accurate numerical results can be obtained with short elapse time.

Applying the present computational method to multiple problems, it will be confirmed that the present computational method allows us to predict the one- to three-dimensional shock-wave problems with high Mach numbers as well as the natural convection flows with low Mach numbers.

Numerical procedures

Governing Equations

The governing equations are the conservation for mass, momentum and internal energy. In Cartesian coordinate system they are given by

$$\frac{\partial \rho}{\partial t} + \frac{\partial (\rho u_j)}{\partial x_j} = 0 \tag{1}$$

$$\frac{\partial (\rho u_i)}{\partial t} + \frac{\partial (\rho u_i u_j)}{\partial x_j} = -\frac{\partial p}{\partial x_j} + \frac{\partial \tau_{ij}}{\partial x_j} - \rho g \delta_{i3} \tag{2}$$

$$\frac{\partial (\rho e)}{\partial t} + \frac{\partial (\rho e u_j)}{\partial x_j} = -p\frac{\partial u_i}{\partial x_i} + \tau_{ij}\frac{\partial u_i}{\partial x_j} - \frac{\partial q_j}{\partial x_j} \tag{3}$$

where ρ, u_i, p, τ_{ij}, g, δ_{ij}, q_i are the density, the velocity component in the x_i direction, pressure, viscous stress tensor, gravity, Kronecker's delta and the heat flux in the x_j direction, respectively. The x_3 coordinate towards the vertically upward direction.

In the above equations, the relationship between the internal energy e and the temperature T is given by

$$e = C_v T \tag{4}$$

where C_v is the specific heat at constant volume. The equation of state for ideal gasses is given by

$$p = \rho e(\gamma - 1) \tag{5}$$

where the γ is the ratio of specific heat. The viscous stress τ_{ij} and the heat flux q_j are defined as

$$\tau_{ij} = \mu\left(\frac{\partial u_i}{\partial x_j} + \frac{\partial u_j}{\partial x_i}\right) - \lambda\frac{\partial u_k}{\partial x_k}\delta_{ij} \tag{6}$$

$$q_j = -\kappa\frac{\partial T}{\partial x_j} \tag{7}$$

where $\lambda = -(2/3)\mu$ and κ is the coefficient of thermal conductivity.

Computational Method for Governing Equations

As shown in Fig.1, the governing equations are discretized on the collocated grid points in the cell where Q denotes the scalar variables. The numerical procedure is given as follows:

1). The tentative velocity components u_i^* are calculated at the cell-center points without pressure-gradient terms.

2). The pressure-gradient terms are added to the velocity components after the interpolation of $u_{b,i}$ on cell boundaries. The cell-boundary velocity components, including the pressure gradient terms, are denoted by $u_{b,i}^*$.

3). The density ρ^{n+1} at $n+1$ time step is calculated from Eq.(1) with the implicit method as detailed later.

4). $(\rho T)^{n+1}$ is calculated from Eqs.(3) and (4) with the implicit method as well. The temperature T^{n+1} is determined with the ρ^{n+1}.

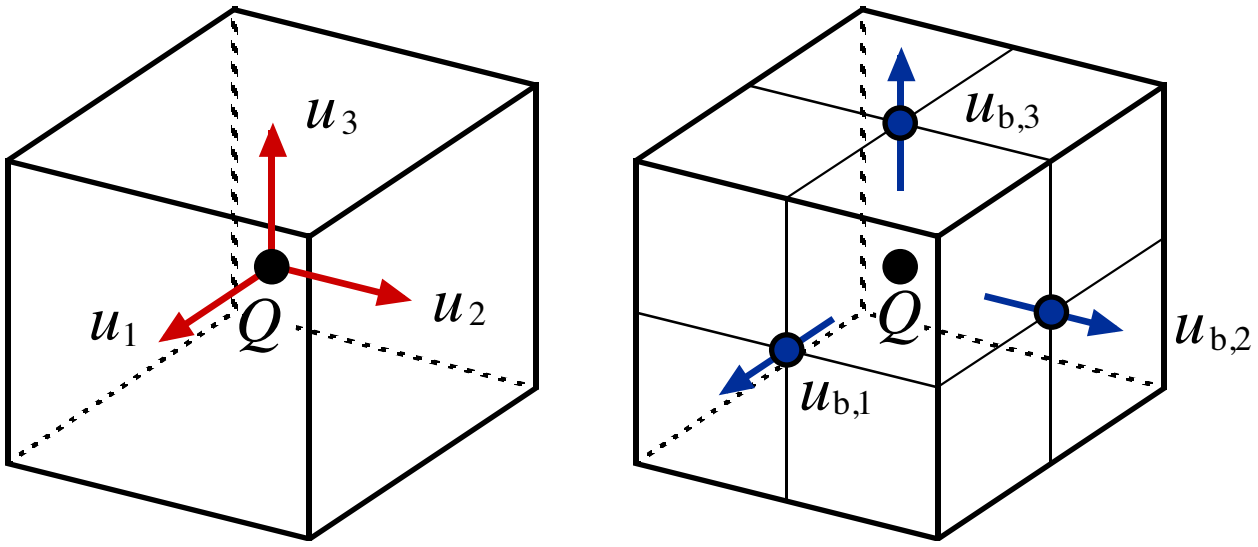

Figure 1. Collocated grid system

5). The pressure p^{n+1} is obtained by Eqs.(4) and (5) with ρ^{n+1} and T^{n+1}. Thus, the equation of state is satisfied by all variables at $n+1$ time step.

6). The momentum $(\rho u_i)^{n+1}$ is calculated from Eq.(2) with the implicit method using the variables at $n+1$ time step. The velocity u_i^{n+1} is determined with ρ^{n+1}.

The details of the above numerical procedures are as follows: the tentative velocity component u_i^* is calculated at the center of the cells with FVM:

$$u_i^* = \frac{1}{\rho^n}\left[(\rho u_i)^n + \Delta t\left\{-\left(\frac{\partial(\rho u_i u_j)}{\partial x_j}\right)^n + \left(\frac{\partial \tau_{ij}}{\partial x_j}\right)^n\right\}\right] \tag{8}$$

where superscripts denote the time step. In order to estimate pressure-gradient terms accurately, these terms are not included in the estimation of u_i^* at the cell-center points.

After this procedure, the pressure-gradient terms estimated on the cell boundaries are added to the interpolated velocity. Thus, we obtain the cell-boundary velocity component $u_{b,i}^*$ as follows:

$$u_{b,i}^* = f_b(u_i^*) - \frac{1}{\rho^n}\frac{\partial p^n}{\partial x_i}\bigg|_b \Delta t \tag{9}$$

where $f_b()$ denotes the function to interpolate the variable on a cell boundary, which is a simple linear average between the cell-center variables in the present paper.

Equation (1) is discretized with the implicit method called C-ISMAC method [Ushijima and Nezu (2002)] proposed for the collocated grid system, which is based on the implicit SMAC method [Shin et al. (1993)] in the staggered grid system. The C-ISMAC method allows us to decrease computational time without decreasing numerical accuracy.

The equation discretized with respect to time by the C-ISMAC method is given by

$$\frac{\rho^{n+1}-\rho^n}{\Delta t} + \alpha_\rho \frac{\partial(\rho^{n+1}u^*)}{\partial x_j} + (1-\alpha_\rho)\frac{\partial(\rho^n u_j^*)}{\partial x_j} = 0 \tag{10}$$

where α_ρ is a parameter whose range is $0 \le \alpha_\rho \le 1$. With the following definition,

$$\rho^{n+1} = \rho^n + \tilde{\rho} \tag{11}$$

Eq.(10) is transformed to the following equation:

$$\frac{\tilde{\rho}}{\Delta t} + \alpha_\rho \frac{\partial(\tilde{\rho} u_j^*)}{\partial x_j} = -\frac{\partial(\rho^n u_j^*)}{\partial x_j} \tag{12}$$

where $\tilde{\rho}$ becomes nearly zero when the flow field is almost steady or the time-scale of the flow field is sufficiently larger than the time increment Δt. Thus, we can apply a simple first-order spatial discretization method to the left-hand side of Eq.(10), while higher-order scheme to the right-hand side. After solving the simultaneous linear equations of $\tilde{\rho}$, which is derived from the discretized equation of Eq.(12) with respect to space, ρ^{n+1} can be obtained from Eq.(11).

With Eq.(4) in which C_v is assumed to be constant, Eq.(3) is rewritten as

$$\frac{\partial(\rho T)}{\partial t}+\frac{\partial\{(\rho T)u_j\}}{\partial u_j}=-(\rho T)(\gamma-1)\frac{\partial u_i}{\partial x_i}+\frac{1}{C_v}\left\{\tau_{ij}\frac{\partial u_i}{\partial x_j}+\frac{\partial}{\partial x_j}\left(\kappa\frac{\partial T}{\partial x_j}\right)\right\} \tag{13}$$

Similarly, the equation discretized by the C-ISMAC method is given by

$$\begin{aligned}\frac{(\rho T)^{n+1}-(\rho T)^n}{\Delta t}&+\alpha_{\rho T}\frac{\partial\{(\rho T)^{n+1}u_j^*\}}{\partial x_j}+(1-\alpha_{\rho T})\frac{\partial\{(\rho T)^n u_j^*\}}{\partial x_j}\\&=(\gamma-1)\left[\beta_{\rho T}\left\{-(\rho T)^{n+1}\frac{\partial u_j^*}{\partial x_j}\right\}+(1-\beta_{\rho T})\left\{-(\rho T)^n\frac{\partial u_j^*}{\partial x_j}\right\}\right]\\&\quad+\frac{1}{C_v}\left\{\tau_{ij}\frac{\partial u^*}{\partial x_j}+\frac{\partial}{\partial x_j}\left(\kappa\frac{\partial T^n}{\partial x_j}\right)\right\}\end{aligned} \tag{14}$$

where $\alpha_{\rho T},\beta_{\rho T}$ are parameters whose ranges are $0\le\alpha_{\rho T},\beta_{\rho T}\le 1$. With the following definition,

$$(\rho T)^{n+1}=(\rho T)^n+(\tilde{\rho T}) \tag{15}$$

Eq.(14) is transformed to the following equation:

$$\begin{aligned}\frac{(\tilde{\rho T})}{\Delta t}&+\alpha_{\rho T}\frac{\partial\{(\tilde{\rho T})u_j^*\}}{\partial x_j}+\beta_{\rho T}(\gamma-1)\left\{(\tilde{\rho T})\frac{\partial u_i^*}{\partial x_i}\right\}\\&=-\frac{\partial\{(\rho T)^n u_j^*\}}{\partial x_j}+(\gamma-1)\left\{-(\rho T)^n\frac{\partial u_j^*}{\partial x_j}\right\}+\frac{1}{C_v}\left\{\tau_{ij}\frac{\partial u_j^*}{\partial x_j}+\frac{\partial}{\partial x_j}\left(\kappa\frac{\partial T^n}{\partial x_j}\right)\right\}\end{aligned} \tag{16}$$

After solving the simultaneous linear equations of $(\tilde{\rho T})$, which is derived from the discretized equation of Eq.(16) with respect to space, we obtain $(\rho T)^{n+1}$ with Eq.(15).

With the similar procedures, Eq.(2) discretized with respect to time is given by

$$\frac{(\rho u_i)^{n+1}-(\rho u_i)^n}{\Delta t}+\alpha_{\rho u_i}\frac{\partial\{(\rho u_i)^{n+1}u_j\}}{\partial x_j}+(1-\alpha_{\rho u_i})\frac{\partial\{(\rho u_i)^n u_j\}}{\partial x_j}=-\frac{\partial p^{n+1}}{\partial x_i}+\frac{\partial\tau_{ij}}{\partial x_j}-\rho^{n+1}g\delta_{i3} \tag{17}$$

where $\alpha_{\rho u_i}$ is a parameter whose range is $0\le\alpha_{\rho u_i}\le 1$. The component $(\rho u_i)^{n+1}$ is defined by

$$(\rho u_i)^{n+1}=(\rho u_i)^n+(\tilde{\rho u_i}) \tag{18}$$

Substituting Eq.(18) into Eq.(17), we have

$$\frac{(\tilde{\rho u_i})}{\Delta t}+\alpha_{\rho u_i}\frac{\partial\{(\tilde{\rho u_i})u_j^*\}}{\partial x_j}=-\frac{\partial\{(\rho u_i)^n u_j^*\}}{\partial x_j}-\frac{\partial p^{n+1}}{\partial x_i}+\frac{\partial\tau_{ij}}{\partial x_j}-\rho^{n+1}g\delta_{i3} \tag{19}$$

After solving the simultaneous linear equations of $(\tilde{\rho u_i})$, which is derived from the discretized equation of Eq.(19) with respect to space, we obtain $(\rho u_i)^{n+1}$ with Eq.(18).

Applicability of the Numerical Method

Sod's Shock Tube Problem

Firstly, the present computational method was applied to one dimensional Sod's shock tube problem [Sod (1978)], in order to confirm that the method is able to capture discontinuity of the variables. Figure 2 shows the initial conditions on the rectangular domain with $l_1 = 0.3$ [m] and $l_2 = 1.0$ [m]. A diaphragm at $x_2 = 0.5$ [m] separates two regions which have different densities and pressures.

The two regions are initially in a static state. The variables in the initial conditions are given as follows:

$$\left.\begin{array}{lll} \rho_L = 1.0\,[\mathrm{kg/m^3}] & , & \rho_R = 0.125\,[\mathrm{kg/m^3}], \\ u_L = 0.0\,[\mathrm{m/s}] & , & u_R = 0.0\,[\mathrm{m/s}], \\ p_L = 1.0\,[\mathrm{Pa}] & , & p_R = 0.1\,[\mathrm{Pa}], \end{array}\right\} \tag{20}$$

where subscripts L and R denote the values on the left and right sides of the diaphragm respectively. T_L and T_R are determined by the equation of state. The ratio of specific heats γ is chosen to be 1.4 assuming that γ of the gas is similar to that of air. The specific heat at constant volume $C_v = 7.17 \times 10^2$ [J/(kg·K)]. The coefficient of thermal conductivity $\kappa = 0$ [W/(m·K)]. The coefficient of viscosity $\mu = 0$ [Pa·s] and the effect of gravity is negligible.

The boundary conditions are given as follows: A free-slip boundary condition is imposed on the top and bottom walls and a non-slip boundary condition is imposed on the left and right walls. On all walls, Neumann boundary conditions are employed: $\partial T/\partial n = 0$, $\partial P/\partial n = 0$ and $\partial \rho/\partial n = 0$.

In the computations, the time step Δt is 4.0×10^{-4} [s] and the number of computational cells is 102×1502. All convection terms on the right-hand side in Eqs.(12), (16) and (19) are evaluated with the third-order MUSCL TVD scheme [Yamamoto and Daiguji(1993)].

Figure 3 shows the dimensionless mass error $err = (M_0 - M')/M_0$ at $t = t'$ [s]. Here M_0 and M' denote the total mass at $t = 0$ [s] and at $t = t'$ [s], respectively. It was shown that the mass conservation law is satisfied accurately in the present computational method.

The numerical results at $t = 0.2$ [s] are shown in Fig.4, in which internal energy e is given by Eq.(4). While the calculated internal energy in the range of $0.68 \leq x_2 \leq 0.85$ is somewhat smaller than the theoretical values, the other predicted results reasonably agree with the exact solutions. Thus, it was shown that the numerical method is applicable to the one-dimensional shock wave problem and that it is able to capture discontinuity without artificial viscosity.

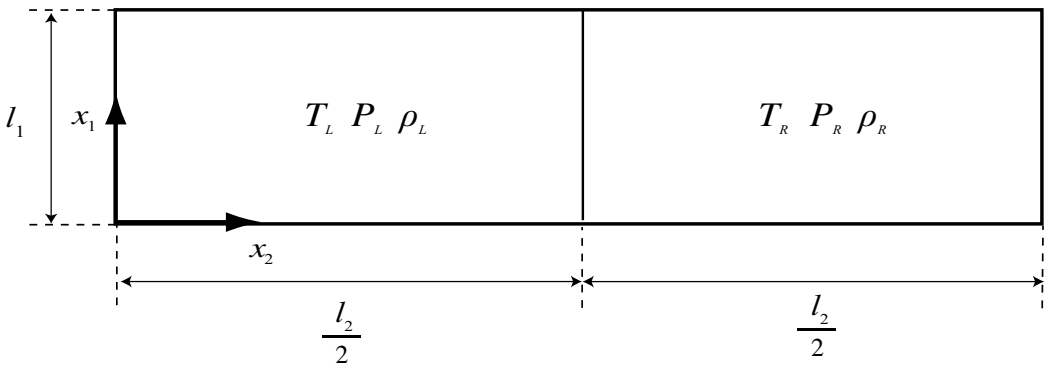

Figure 2. Initial conditions for Sod's shock tube problem

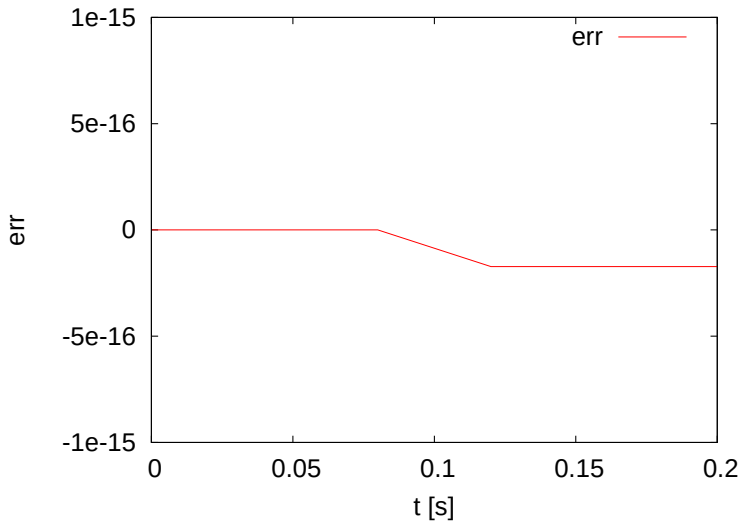

Figure 3. Dimensionless mass error

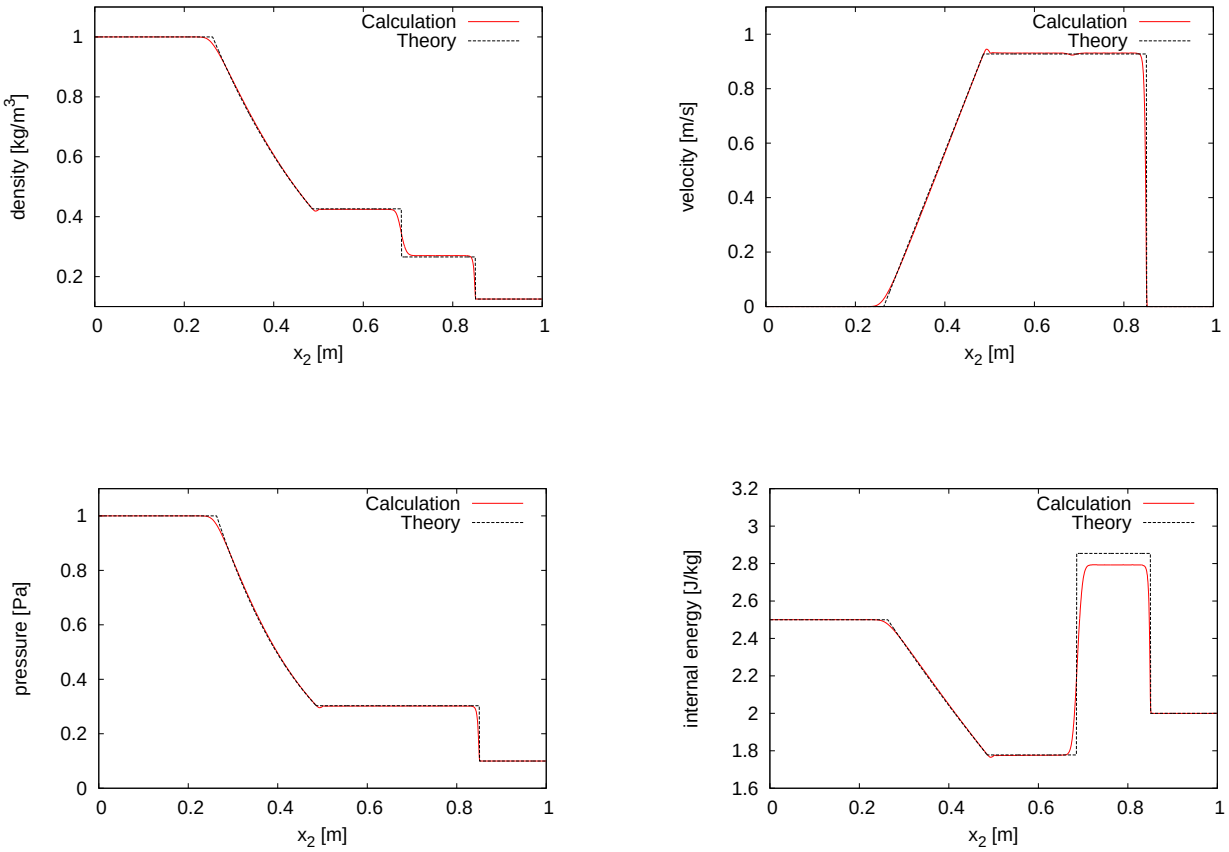

Figure 4. Numerical results ($x_1 = 0.5 l_1$ **and** $t = 0.2$ **[s])**

Secondary, the present computational method was applied to the two-dimensional problem in the square domain of $l_1 = l_2 = 2.0$ [m], including a circular area at its center, as shown in Fig.5. The initial conditions are different between the circular region, whose radius r is 0.4 [m], and the region outside the circle.

The flow is in a static condition in all regions at $t = 0$ [s]. The initial conditions are given as follows:

$$\left.\begin{array}{lcl} \rho_{in} = 1.0\,[\mathrm{kg/m^3}] & , & \rho_{out} = 0.125\,[\mathrm{kg/m^3}], \\ u_{1in} = 0.0\,[\mathrm{m/s}] & , & u_{1out} = 0.0\,[\mathrm{m/s}], \\ u_{2in} = 0.0\,[\mathrm{m/s}] & , & u_{2out} = 0.0\,[\mathrm{m/s}], \\ p_{in} = 1.0\,[\mathrm{Pa}] & , & p_{out} = 0.1\,[\mathrm{Pa}], \end{array}\right\} \tag{21}$$

where subscripts *in* and *out* denote the values inside and outside the circle respectively. T_{in} and T_{out} are given by the equation of state. The ratio of specific heats γ was chosen to be 1.4 assuming that air behaves as an ideal gas. The coefficient of thermal conductivity $\kappa = 0$ [W/(m·K)]. The coefficient of viscosity $\mu = 0$ [Pa·s]. The time step Δt is 5.0×10^{-4} [s] and the effects of gravity is also negligible.

The boundary conditions are given as follows: A free-slip boundary condition is imposed on all walls. On all walls, $\partial T/\partial n = 0$, $\partial P/\partial n = 0$ and $\partial \rho/\partial n = 0$.

All convection terms on the right-hand side in Eqs.(12), (16), and (19) are evaluated with the third-order MUSCL TVD scheme [Yamamoto and Daiguji(1993)].The number of computational cells is 1002×1002.

The predicted results at $t = 0.25$ [s] are shown in Figs. 6, 7 and 8. As shown in Figs. 6 and 7, the density and pressure distributions qualitatively agree with the predicted values of [Toro(1997)]. Figure 8 shows a comparison between the present numerical results and the analytical solutions of [Toro(1997)]. While only the internal energy e in the range of $1.62 \leq x_1 \leq 1.81$ is smaller than the analytical solution, the other numerical results reasonably agree with the reference values. From the above results, it can be seen that the present numerical method is also applicable to two-dimensional problems.

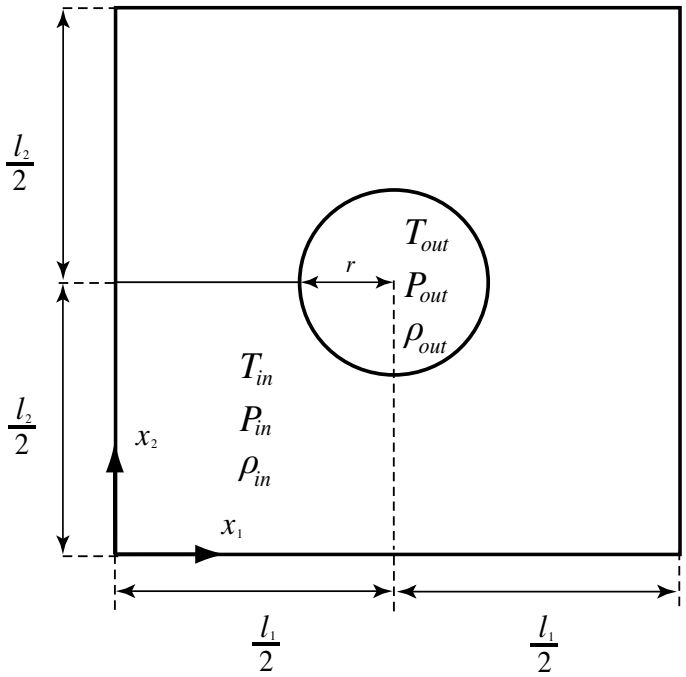

Figure 5. Initial conditions for cylindrical explosion

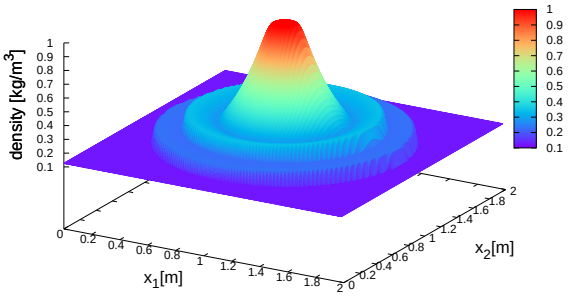

Figure 6. Density distribution at $t = 0.25$ [s]

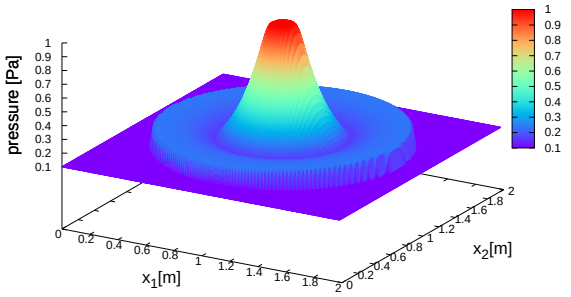

Figure 7. Pressure distribution at $t = 0.25$ [s]

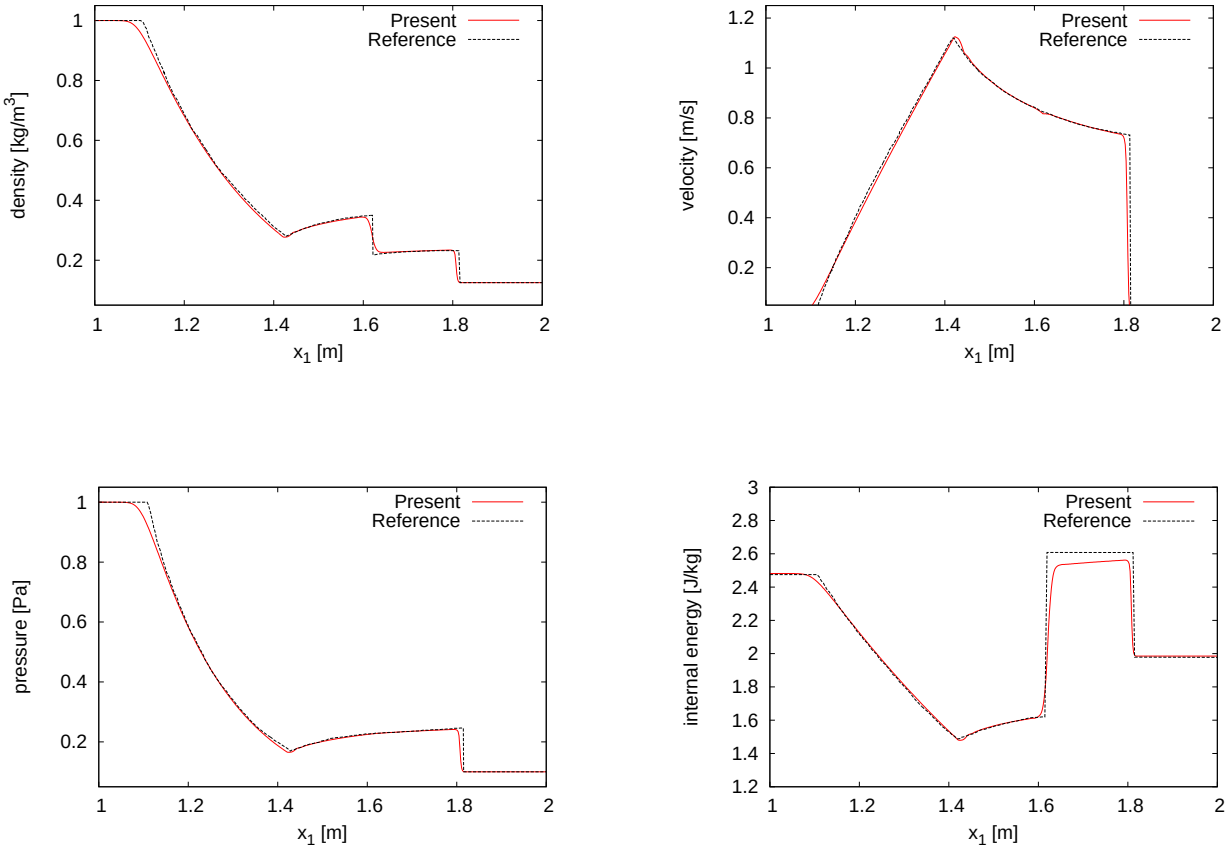

Figure 8. Numerical results and reference values [Toro(1997)] ($x_2 = 0.5l_2$ and $t = 0.25$ [s])

As the final example of the high Mach number flows necessary to be solved by the large scale computations, the present computational method was applied to the three-dimensional shock-wave problem in the cubic domain with $l_1 = l_2 = l_3 = 2.0$[m], including a spherical region located in its center, as shown in Fig.9.

The initial conditions ($t = 0$ [s]) in the sphere of radius $r = 0.4$ [m] and the region outside the sphere are given the same as the two-dimensional case listed in Eq. (21). In addition, the physical properties and the gravity effects are also treated in the same way as the two-dimensional problem. The initial x_3 velocity components are set at $u_{3in} = u_{3out} = 0$ [m/s].

Th boundary conditions are given as follows: A free-slip boundary condition is imposed on all walls. On all walls, $\partial T/\partial n = 0$, $\partial P/\partial n = 0$ and $\partial \rho/\partial n = 0$.

All convection terms on the right-hand side in Eqs.(12), (16) and (19) are evaluated with the fifth-order compact upwind TVD scheme [Yamamoto and Daiguji(1993)].The time step Δt is 1.0×10^{-4} [s]. The number of computational cells is $802 \times 802 \times 802$. In order to solve this large scale problem efficiently, the computation was parallelized by flat MPI on the basis of a domain decomposition method.

Figure 10 shows a comparison between the present numerical results at $t = 0.25$ [s] and the analytical solutions of [Toro(1997)]. While some discrepancies are found in the distribution of the internal energy e in the range of $1.61 \leq x_1 \leq 1.79$ and near the discontinuous distributions of density and pressure compared with the analytical solution, the outline of the predicted results reasonably agree with the reference values. Therefore, it was shown that the present numerical method can be applied to three-dimensional problems as well.

In addition, the efficiency of the parallel computations was examined by changing the core numbers. Fig.11 shows the speed-up ratios on the basis of 32 cores in the Cray-XE6 in Kyoto University (AMD Opteron 2.5GHz, 32 cores / node, 64 GB memory / node). The maximum core number is 512 (16 nodes). As shown in Fig.11, the tendency of the increasing speed-up ratio is near the linear line. Thus, the present flat MPI parallelization enables us to decrease the elapse time satisfactorily.

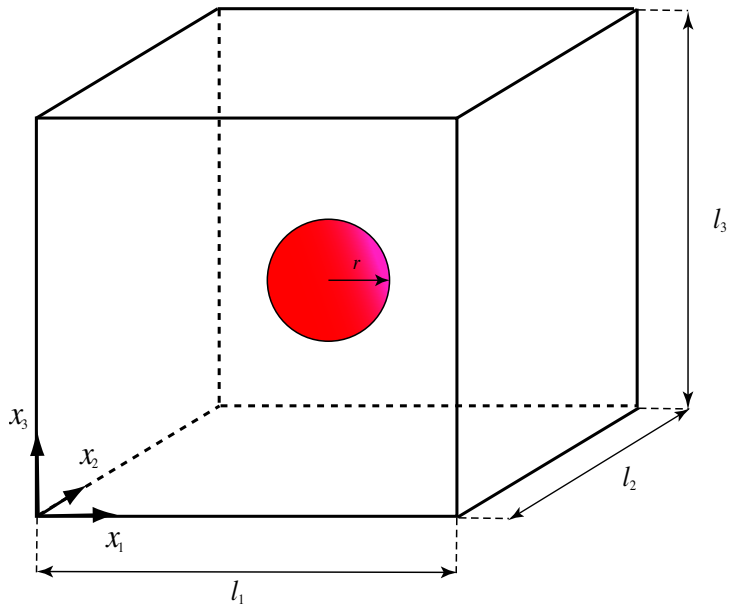

Figure 9. Calculation area for spherical explosion

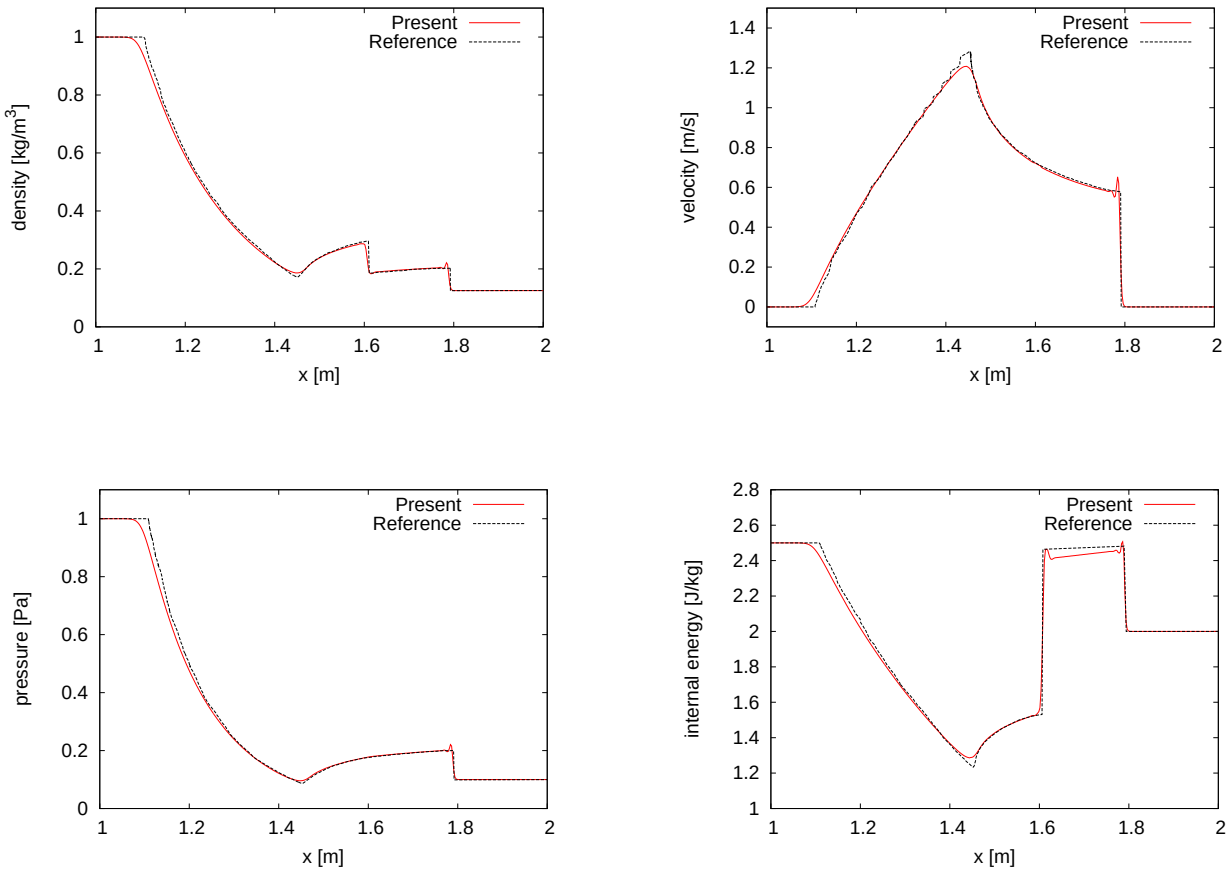

Figure 10. Numerical results (at $t = 0.25$ [s])

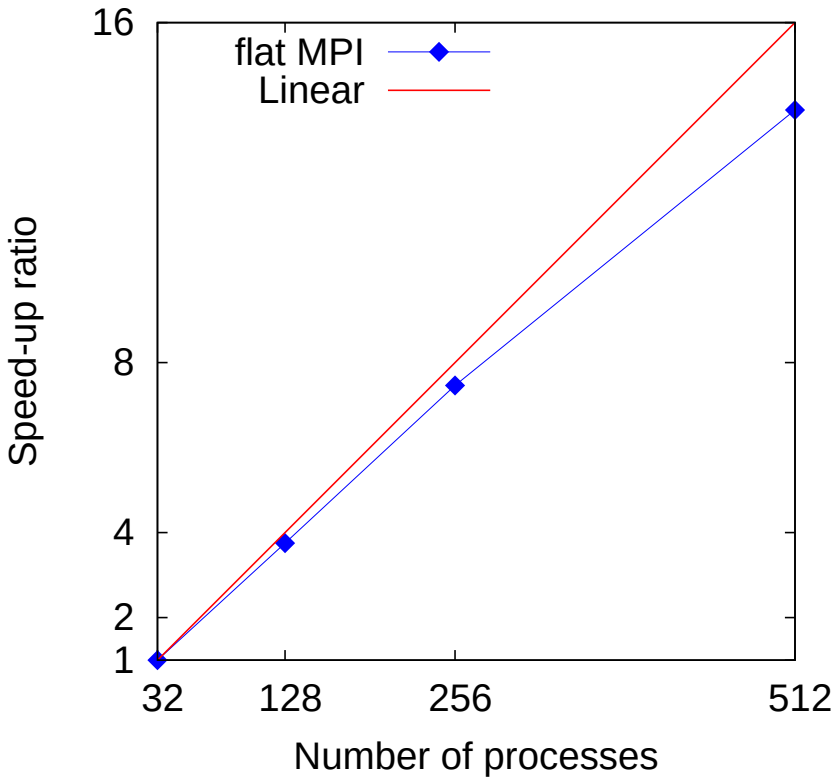

Figure 11. Speed-up ratios of flat MPI

On the other hand, in order to confirm the applicability of the present method to the flows with low Mach numbers, it was applied to the natural convection in a square cavity with differentially heated side walls. While the compressibility is not so dominant in the example employed in this section, this is a suitable benchmark problem to confirm the applicability of the computational method.

As shown in Fig.12, the computational domain is a square cavity including the fluid of Prandtl number $Pr = 0.71$. The length of the square cavity is $l_1 = l_3 = 0.1$[m]. The acceleration of gravity affects in $-x_3$ direction. The the Rayleigh number Ra and Prandtl number Pr are defined as

$$Ra = \frac{Bg\Delta T l_3^3}{A\nu} \tag{22}$$

$$Pr = \frac{\nu}{A} \tag{23}$$

where A, B, μ, ν are thermal diffusivity, coefficient of thermal expansion, viscosity and kinematic viscosity, respectively.

The dimensionless numbers and the average Nusselt number are defined as

$$T^* = \frac{T_{cal} - T}{\Delta T} \quad , \quad x_1^* = \frac{x_1}{l_3} \quad , \quad x_3^* = \frac{x_3}{l_3}, \quad , \quad u_1^* = \frac{u_1 l_3}{A} \quad , \quad u_3^* = \frac{u_3 l_3}{A} \tag{24}$$

$$\overline{Nu} = \frac{1}{l_3}\int_0^{l_3} Nu\, dx_3 \Big|_{x_3=0\ or\ 0.1} \tag{25}$$

where T_{cal} is the predicted results of the temperature.

The initial conditions are given as follows: the velocity component u_i and the temperature T are set to zero and 300 [K] in the cavity. The pressure is set by considering gravity and the density is given by the equation of state with the initial pressure, temperature, the ratio of specific heats $\gamma = 1.4$.

The boundary conditions are given as follows: A non-slip boundary condition is imposed on all walls. $T = 300 + \Delta T$ [K] at $x_1 = 0$ [m] and $T = 300$ [K] at $x_1 = 0.1$ [m] where $\Delta T = 1$ [K]. The boundaries at $x_3 = 0$ [m] and 0.1 [m] are adiabatic, $\partial T/\partial x_3 = 0$ and $\partial \rho/\partial x_3 = 0$. On the vertical walls $\partial p/\partial x_1 = 0$, while p is set by considering gravity on the horizontal walls.

In the computations, The time step Δt is 8.0×10^{-7} [s]. The number of computational cells is 152×152. The predicted results were obtained at two Rayleigh numbers: $Ra = 10^4$ and 10^5. The coefficient of thermal conductivity $\kappa = 7.63467 \times 10^{-2}$ [W/(m·K)] and the coefficient of viscosity $\mu = 5.42061 \times 10^{-5}$ [Pa·s] at $Ra = 10^4$, while $\kappa = 2.41429 \times 10^{-2}$ [W/(m·K)] and $\mu = 1.71414 \times 10^{-5}$ [Pa·s] at $Ra = 10^5$.

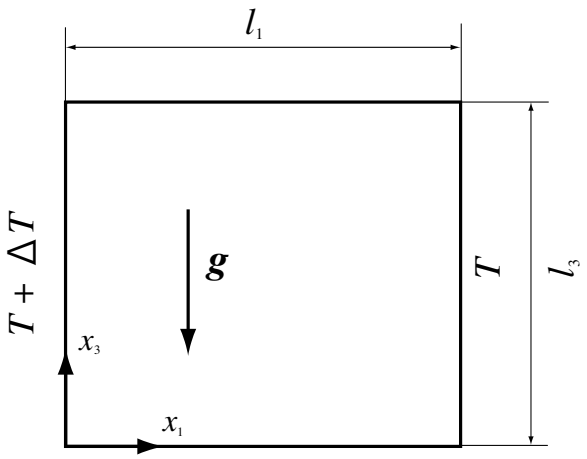

Figure 12. Calculation area for natural convection

Figures 13 and 14 show the calculated results with the present method. As shown in Figs.13 and 14, the isotherms and the isovels at steady state qualitatively agree with the predicted values of [Davis(1983)].

Table 1 shows the magnitude and the location of the maximum velocity u^*_{1max} along the vertical centerline, the maximum velocity u^*_{3max} along the horizontal centerline and the average Nusselt number $\overline{Nu}$ for Ra of 10^4 and 10^5. In Table1, the predicted results are compared with the benchmark results of [Davis and Jones(1983)] and [Dixit and Babu(2006)]. While u^*_{1max} at $Ra = 10^5$ at steady state is larger than that of [Davis and Jones(1983)], the other results reasonably agree with them.From these results, in addition to the high Mach number flows as shown in the above sections, it was shown that the present numerical method enables us to deal with the flows in low Mach numbers affected by viscosity and thermal diffusivity. It can be concluded that the numerical algorithm proposed in this paper is widely applicable to the flows from low to high Mach numbers.

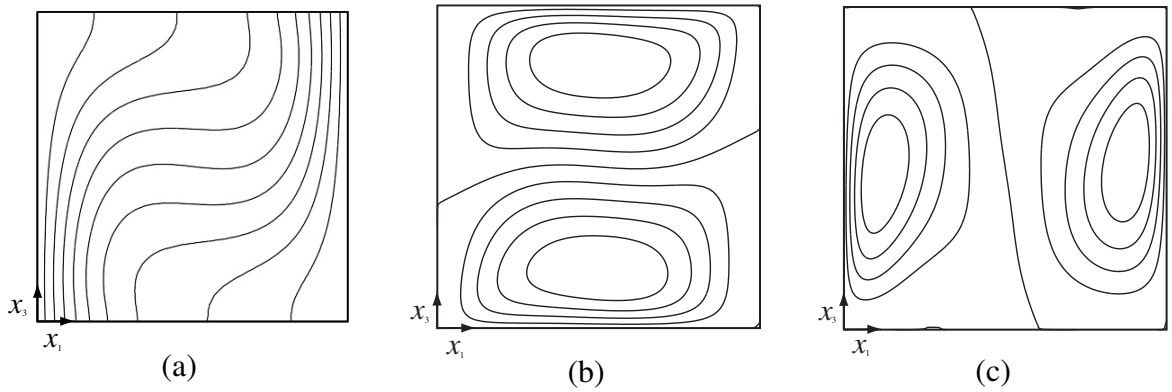

Figure 13. Contour maps for predicted results at $Ra = 10^4$: (a) T^*, (b) u^*_1, (c) u^*_3

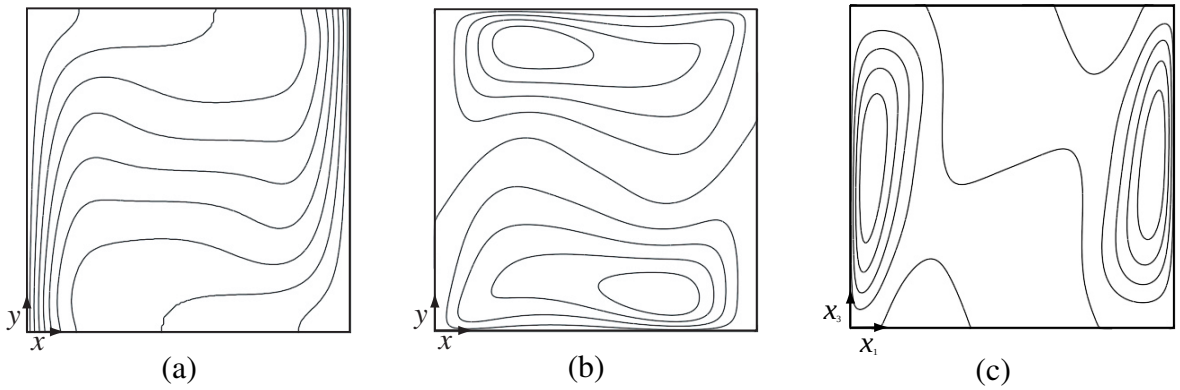

Figure 14. Contour maps for predicted results at $Ra = 10^5$: (a) T^*, (b) u^*_1, (c) u^*_3

Table 1. Comparison among numerical results

	Present		[Davis and Jones(1983)]		[Dixit and Babu(2006)]
Ra	10^4	10^5	10^4	10^5	10^4
u^*_{1max}	16.193	43.87	16.178	34.73	16.179
x^*_3	0.823	0.890	0.823	0.855	0.824
u^*_{3max}	19.649	68.52	19.617	68.59	19.619
x^*_1	0.117	0.063	0.119	0.066	0.121
$\overline{Nu}$	2.245	4.528	2.243	4.519	2.245

Conclusions

In this paper, the computational algorithms and numerical discretizations were newly proposed for governing equations of compressible fluids in an attempt to establish the numerical method which can be widely applicable to the flows from low to high Mach number. In this method, some numerical techniques proposed for the incompressible fluids are utilized on the collocated grid system on the basis of FVM. As a result, the conservation of variables are satisfied and the equation of state is established for $n+1$ time step variables. In addition, the parallelization with the domain decomposition method is easily employed due to the collocated grid system.

As a result of the computation of some benchmark problems, it has been shown that the present computational method enables us to capture shock discontinuity without artificial viscosity. It was also confirmed that the present method is applicable to the natural convection flow with low Mach number affected by viscosity and thermal conductivity.

References

S. Ushijima and I. Nezu (2002) Higher-order implicit (C-ISMAC) method for incompressible flows with collocated grid system, *Journal of JSCE*, **719**, 21-30.

B. R. Shin, T.Ikohagi, and H. Daiguji (1993) An unsteady implicit SMAC scheme for two-dimensional incompressible Navier-Stokes equations, *JSME International Journal*, **36**, 598-606

S. Yamamoto and H. Daiguji (1993) Higher-order-accurate upwind schemes for solving the compressible Euler and Navier-Stokes equations, *Computers Fluids*, **22**, 259-270.

Gray A. Sod (1978) A survey of several finite difference methods for systems of nonlinear hyperbolic conservation laws, *Journal of Computational Physics*, **27**, 1-31.

E. F. Toro (1999) *Riemann Solvers and Numerical Methods for Fluid Dynamics*, 2nd edn, Springer-Verlag, Berlin.

G. de Vahl Davis (1983) Natural convection in a square cavity : a bench mark numerical solution, *International Journal for Numerical Methods in Fluids* **3**, 249-264.

G. de Vahl Davis and I. P. Jones (1983) Natural convection in a square cavity : a comparison exercise, *International Journal for Numerical Methods in Fluids*, **3**, 227-248.

H. N. Dixit and V. Babu (2006) Simulation of high Rayleigh number natural convection in a square cavity using the lattice Boltzmann method, *International Journal of Heat and Mass Transfer*, **49**, 727-739.